

# A *Chandra* observation of the disturbed cluster core of Abell 2204

J.S. Sanders<sup>1\*</sup>, A.C. Fabian<sup>1</sup> and G.B. Taylor<sup>2</sup>

<sup>1</sup> *Institute of Astronomy, Madingley Road, Cambridge. CB3 0HA*

<sup>2</sup> *National Radio Astronomy Observatory, P.O. Box 0, Socorro, NM 87801, USA*

15 September 2018

## ABSTRACT

We present results from an observation of the luminous cluster of galaxies Abell 2204 using the *Chandra X-ray Observatory*. We show the core of the cluster has a complex morphological structure, made up of a high density core ( $n_e \sim 0.2 \text{ cm}^{-3}$ ) with flat surface brightness, a surrounding central plateau, a tail-like feature, wrapping around to the east, and an unusual radio source. A temperature map and deprojected-profile shows that the temperature rises steeply outside these regions, until around  $\sim 100$  kpc where it drops, then rises again. Abundance maps and profiles show that there is a corresponding increase in abundance at the same radius as where the temperature drops. In addition there are two cold fronts at radii of  $\sim 28$  and  $54.5$  kpc. The disturbed morphology indicates that the cluster core may have undergone a merger. However, despite this disruption the mean radiative cooling time in the centre is short ( $\sim 230$  Myr) and the morphology is regular on large scales.

**Key words:** X-rays: galaxies — galaxies: clusters: individual: Abell 2204

## 1 INTRODUCTION

The cluster of galaxies Abell 2204 lies at a redshift of 0.1523. It is luminous ( $L_X = 2 \times 10^{45} h_{50}^{-2} \text{ erg s}^{-1}$  in the 2–10 keV band; Edge et al 1990). Schuecker et al (2001) and Buote & Tsai (1996) found this cluster had a regular morphology based on *ROSAT* data.

Peres et al (1998) identified this cluster as having the second most massive cooling flow within the brightest 50 galaxy clusters. In post-*Chandra/XMM-Newton* times this means it has a highly peaked soft X-ray surface brightness profile. Using a constant-pressure cooling flow spectral model Allen (2000) found a best-fitting cooling flow flux value of  $2103_{-378}^{+356} M_{\odot} \text{ yr}^{-1}$ . The central galaxy of Abell 2204 is one of the strongest optical line emitters within a redshift of 0.2, with much massive star formation (Crawford et al 1999), CO line emission (Edge 2001) and  $\text{H}_2$  line emission (Edge et al 2002), indicating the presence a significant mass of cold gas near the centre.

Jenner (1974) found that the two optical nuclei of this cluster differ in velocity by  $249 \text{ km s}^{-1}$ . Clowe & Schneider (2002) detected weak lensing gravitational shear around Abell 2204 at high significance, whilst Dahle et al (2002) observed around a dozen red and blue arcs and arclets surrounding the central cluster galaxy, and found the mass distribution to be elongated in the east-west direction.

Distances in this paper assume a cosmology with  $H_0 = 70 \text{ km s}^{-1} \text{ Mpc}^{-1}$  and  $\Omega_{\Lambda} = 0.7$ . With this cosmology, 1 arcsec corresponds to a distance of 2.6 kpc. The data were processed with version 3.0.2 of CIAO, and the spectra were fit with version 11.3

of XSPEC (Arnaud 1996). We used the solar abundance ratios of Anders & Grevesse (1989). All positions are in J2000 coordinates.

## 2 DATA PREPARATION

Abell 2204 was observed by *Chandra* in 2000-07-29. The data were reprocessed with the latest gain file appropriate for the dataset (`acisD2000-01-29gain_ctiN0001.fits`). Time dependent gain correction was also applied using the `CORR_TGAIN` utility and the November 2003 versions of the correction (Vikhlinin 2003). In addition the CIAO version of the `LC_CLEAN` script (Markevitch 2004) was used to remove periods of the dataset where the count rate was not quiescent. Very little time was removed, producing an event file with an exposure of 10.1 ks. We used a blank sky ACIS background events file (`acis7sD2000-01-29bkgrndN0003.fits`) when fitting the spectra, reprocessed to have the same gain file as the dataset. We checked the count rate in the observation in a 8–10 keV band where there are likely to be very few source photons. It matched the count rate in the blank sky background file to better than 0.5 per cent.

## 3 ANALYSIS

Fig. 1 (top) shows an image of the central region of the cluster using  $\sim 1$  arcsec binning. In Fig. 1 (bottom) we show an image with  $\sim 0.5$  arcsec binning of the innermost core. In these and the other images we present, we have excluded visually identified point sources (Table 1).

\* E-mail: jss@ast.cam.ac.uk

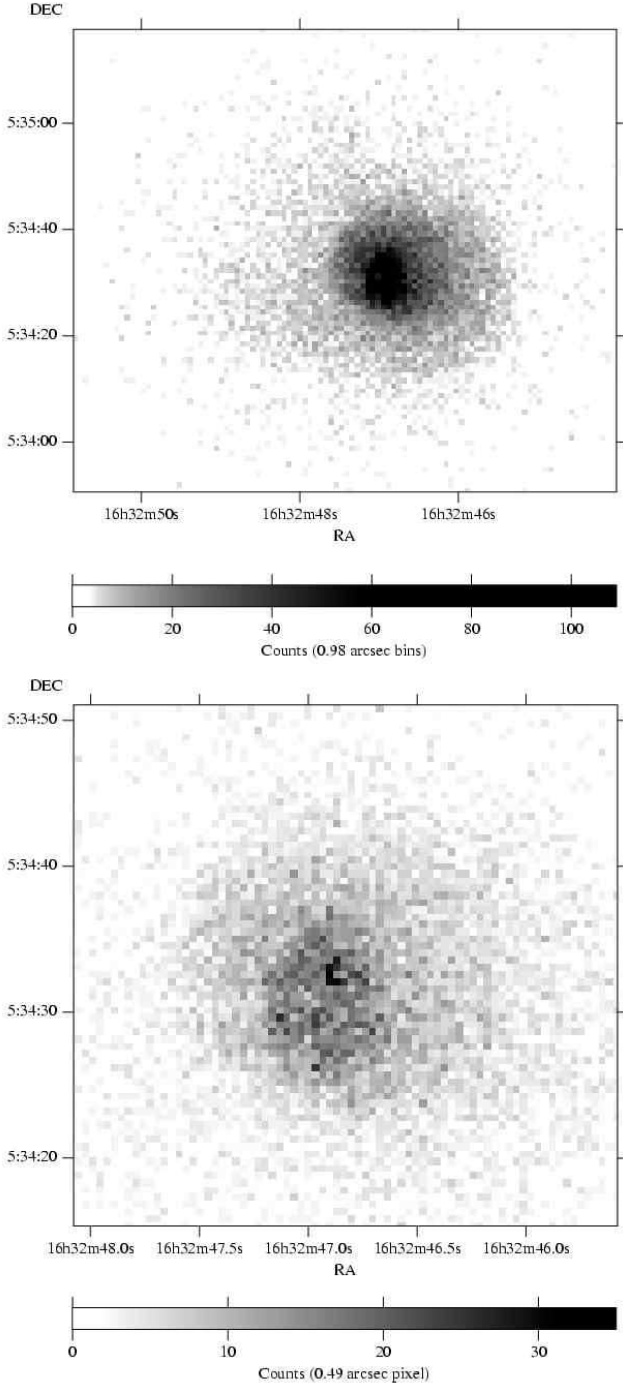


**Figure 1.** (Top) Image of the cluster between 0.5 and 7 keV with 0.98 arcsec bins. (Bottom) Image of the central region with 0.49 arcsec bins.

RA	Dec
16:32:56.8	+05:34:59.9
16:32:51.3	+05:34:53.5
16:32:53.1	+05:32:02.3
16:33:00.2	+05:37:32.9
16:32:58.0	+05:37:38.8

**Table 1.** Excluded point sources (J2000).

Using a smoothed image we defined regions for spectral analysis using a “contour binning” method (Sanders et al, in preparation). The algorithm defines regions with a signal to noise greater than a threshold by “growing bins” in the direction on a smoothed map which has a value closest to the mean value of those pixels already binned. This technique defines bins which are matched to the surface brightness profile of the object. Additionally we applied constraints on the regions to have edge lengths which are 3 times or less than those of circles with the same area, preventing the bins from becoming annular.

The smoothed map was created using an “accumulative smoothing” algorithm (Sanders et al, in preparation), smoothed to have a signal to noise ratio of at least 8. For each pixel, we find the signal to noise ratio. If it is less than a set threshold, we add those pixels of distance  $\leq 1$  pixel from the starting point. We repeat, increasing in radius, until the signal to noise threshold is reached. The value of the smoothed pixel is the average of the pixels summed to reach the signal to noise threshold.

We extracted spectra from the binned spatial regions for the dataset and background dataset. In addition weighted responses (weighted by the number of counts between 0.5 and 7 keV) and ancillary-responses were created for each bin. We fitted the spectra in XSPEC by minimising the C-statistic (Cash 1979). The spectra were not grouped and were fit between 0.6 and 8 keV. The model we fitted to each region was a MEKAL emission spectrum (Mewe, Gronenschild & van den Oord 1985; Liedahl, Osterheld & Goldstein 1995), absorbed by an PHABS absorption model (Balucinska-Church & McCammon 1992). In the fit the temperature, abundance, normalisation, and absorption were free parameters.

The results for the spectral analysis were combined together to form a map. In Fig. 2 (left) we show a temperature map produced by fitting spectra from regions with a signal to noise ratio of  $\geq 40$  ( $\gtrsim 1600$  counts per spectrum), and a profile of the temperatures of each region, plotted by radius from the centre of the cluster. Similarly, in Fig. 2 (right) we show an abundance map and profile.

The centre of the cluster contains an ellipsoidal core of dimensions  $7 \times 9$  arcsec ( $19 \times 24$  kpc) in the east-west and north-south directions. This core has a very flat surface brightness profile (as seen in Fig. 1 [bottom] and Fig. 3). There is a point source offset from the centre of the core to the north-west by 2 arcsec, coincident in position with the edge of the southern lobe of the radio source (See Fig. 4). The projected emission-weighted temperature of the core region is  $3.26 \pm 0.20$  keV with a high abundance of  $1.11 \pm 0.20 Z_{\odot}$  ( $1\sigma$  uncertainties), found using a MEKAL model. From Fig. 2 (right) there are indications that there could be an abundance drop in the very centre. A similar effect is seen in other clusters (e.g. Centaurus – Sanders & Fabian 2002; Abell 2199 – Johnstone et al 2002; Perseus - Sanders et al 2004; Schmidt, Fabian & Sanders 2002; Churazov et al 2003; NGC 4636 – Jones et al 2002). However the evidence is much less significant when we later examine the profile accounting for projection (Fig. 7).

Like most X-ray luminous clusters, Abell 2204 hosts a moderately bright radio source. We obtained short (122 and 30 min) VLA observations of TXS 1630+056 at 1.4 and 5 GHz respectively on 1998 April 23 with the VLA in its A-configuration. In Fig. 4 we show the 1.4 GHz radio image in contours overlaid on the X-ray image. The radio source has an unusual morphology consisting of three components, roughly aligned in the N-S direction over 10 arcsec, with an extension to the west. In addition larger structures are hinted at in the NVSS image (Condon et al 1998). Such a disturbed radio morphology is similar to that seen in the centres of other dense clusters such as PKS 0745-191 (Taylor, Barton & Ge

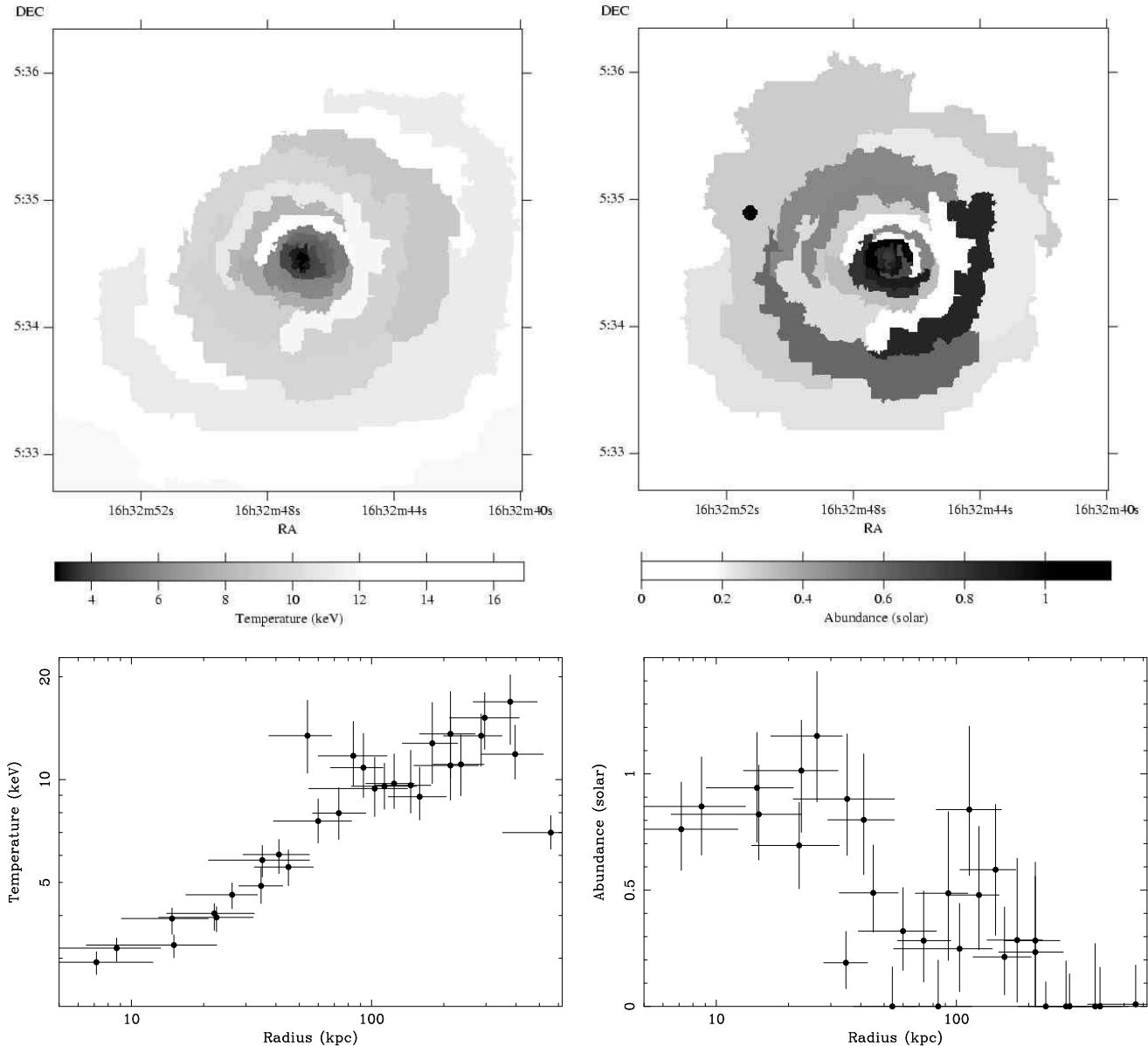


**Figure 2.** Generated maps of the cluster using a signal to noise ratio  $\geq 40$ . (Upper Left) Temperature map of the cluster. (Bottom Left) Temperature profile of the regions in the above map. (Upper Right) Abundance map of the cluster. (Bottom Right) Abundance profile. The points are at the mean radius of each bin, whilst the horizontal error bars indicate the range of radii occupied. The vertical error bars show the  $1\text{-}\sigma$  uncertainties.

1994) and A2052 (Zhao et al. 1993). It is also worth noting that in the 5 GHz VLA observations the brightest component, with a peak flux density of 16 mJy, is  $<0.1\%$  polarised ( $3\sigma$ ). Such a low polarised flux density is also seen in the cluster PKS 0745-191 and is most likely the result of very high Faraday rotation measure gradients produced by a tangled cluster magnetic field (Taylor, Barton & Ge 1994). There are no apparent holes in the X-ray emission corresponding to the main northern radio lobe. This would be the case if the lobe is along the line of sight but not in the X-ray bright ellipsoidal core.

In Fig. 5 we show contours from an accumulatively-smoothed X-ray image of the cluster on an optical image from the *Hubble Space Telescope* (*HST*). There are two closely separated galaxies at the centre of the cluster separated by a distance of 4 arcsec. The northern-most galaxy is associated with the brightest region of emission on the X-ray map in the core (although we find an off-

set of  $\sim 1$  arcsec if the absolute astronomy is correct), whilst the other galaxy to the south-west lies off the core. The northern-most galaxy has a fairly irregular morphology with a strong dust lane extending from close to the core to the south, and other possible regions of absorption lying around its core. It is unclear whether the two galaxies lie in close proximity in the cluster or whether they are only associated by line of sight. However the small velocity difference between the galaxies ( $249\text{ km s}^{-1}$ ; Jenner 1974) suggests that they are closely associated.

The core is embedded in another region with a smooth surface brightness profile and radius  $\sim 10$  arcsec. Within this central plateau the core is displaced to the south. The central plateau has a temperature of  $3.7 \pm 0.2$  keV and an abundance of  $0.85 \pm 0.15 Z_{\odot}$ .

To the north-east of the central plateau there is an abrupt drop in surface brightness by a factor of  $\sim 2.5$ . If we extract and fit projected spectra either side of this jump in brightness, on the inner-

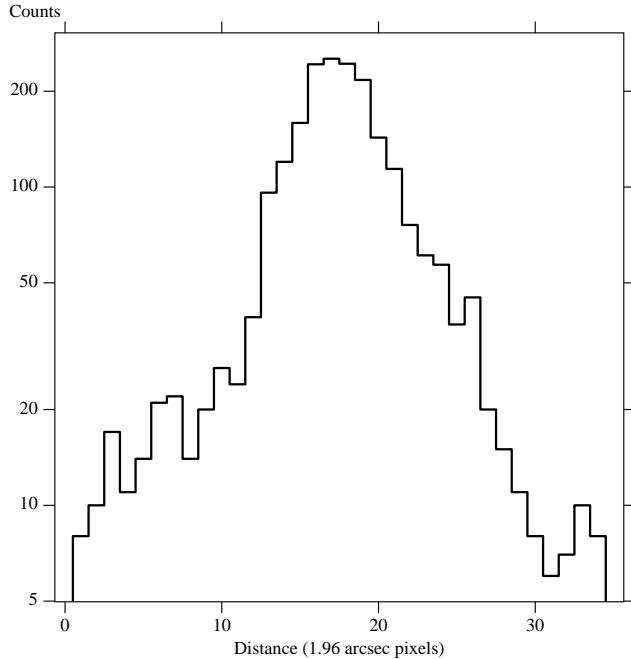


**Figure 3.** Profile over the core of the cluster from the NE to the SW, plotting the number of counts in 1.96 arcsec pixels. The cold fronts are at  $\sim 12$  (NE) and 26 pixels (SW).

most side the gas has a temperature of  $4.1 \pm 0.6$  keV and abundance of  $0.97_{-0.22}^{+0.35} Z_{\odot}$ , but on the outside the temperature is  $9.3_{-2.0}^{+3.0}$  keV, with abundance  $< 0.6$  ( $1-\sigma$ ). Therefore there is a jump in temperature by a factor of  $\sim 2.3$ . We extracted spectra in sectors either side of the drop, and fitted the PROJECT model in XSPEC with an absorbed single temperature MEKAL component. This model accounts for projection by including the contribution of gas lying outside each shell to the spectra. We allowed the temperature, abundance and normalisation of each shell to be free, but tied the absorption to be the same in each shell. Fig. 6 (left) shows the temperature, abundance, density and pressure profiles across the drop (whose radius is marked with a dotted line). It can be seen that although the temperature rises dramatically and the density drops across the drop, the pressure remains constant. Therefore the drop is likely to be a cold front (Markevitch et al 2000).

Extending from the west of the central plateau is a plume-like feature which wraps clockwise around that plateau, decreasing in surface brightness along its length, where the plume merges into the surrounding diffuse emission. The plume is associated with a region of lower temperature on the temperature map. To the west of the plume and core is a significant drop in surface brightness. The temperature beyond the drop is well fitted with a MEKAL model with a temperature of  $10.0_{-1.4}^{+1.8}$  keV, but inside is  $6.6_{-1.0}^{+1.8}$  keV. The surface brightness falls by a factor of 3.6, which is greater than at the previous cold front. We again extracted and fitted spectra in sectors accounting for projection (Fig. 6 [right]). Similarly we found that the pressure across the drop is continuous. Therefore it is likely to be another cold front.

The temperature map and profile (Fig. 2 [left]) indicate that the temperature rises with radius along an approximate power-law until a radius of  $\sim 100$  kpc when it starts to drop back down again, before increasing again at around at  $\sim 200$  kpc. This behaviour is similar to that shown by the abundance map and profile (Fig. 2 [right]). The abundance rises from  $\sim 0.8 Z_{\odot}$  at the centre to  $\sim 1.2 Z_{\odot}$ , then

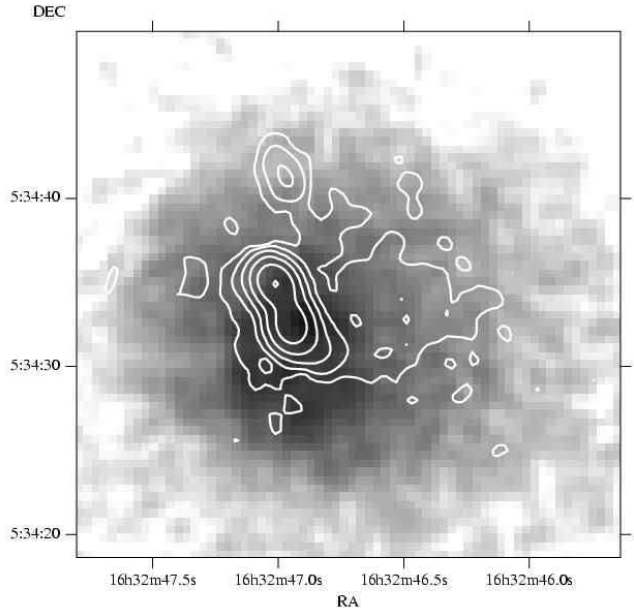


**Figure 4.** X-ray image between 0.5 and 7 keV, smoothed with a Gaussian of 0.49 arcsec, overlaid with contours from a VLA 1.4 GHz radio map of the central radio source. The 6 contours are spaced logarithmically between  $10^{-4}$  and  $0.022$  Jy beam $^{-1}$ . The beam size is  $1.78 \times 1.39$  arcsec in position angle 33 degrees.

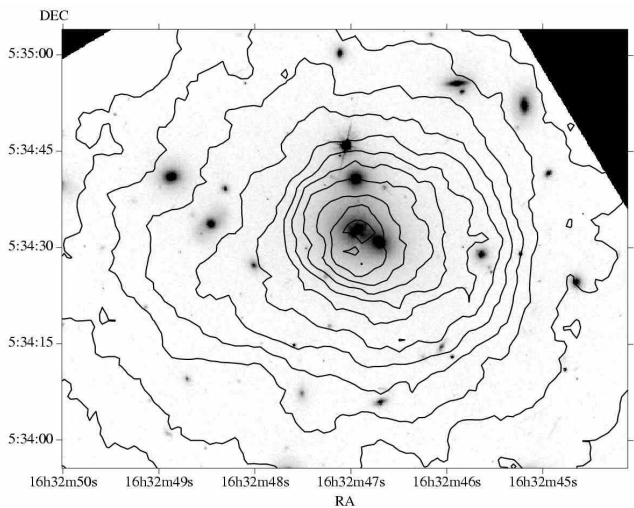


**Figure 5.** *HST* image of the centre of the cluster with accumulated smoothed X-ray contours overlaid. The *HST* image is taken from the WFPC2 Associations catalogue, <http://archive.stsci.edu/hst/wfpc2/> (association name U5A44101B) using the F606W filter. The X-ray image is an accumulated smoothed image between 0.5 and 7 keV with a signal to noise ratio of 10, with 16 contours logarithmically spaced between 0.1 and 24 counts per pixel.

declining steeply with radius. Where the temperature drops down slightly at  $\sim 100$  kpc, the abundance rises up, before falling away again.

In Fig. 7 we show electron density, temperature and abundance profiles made by fitting the PROJECT model in XSPEC with a single temperature MEKAL model, accounting for projection assuming spherical symmetry. We tied the absorption to be the same in

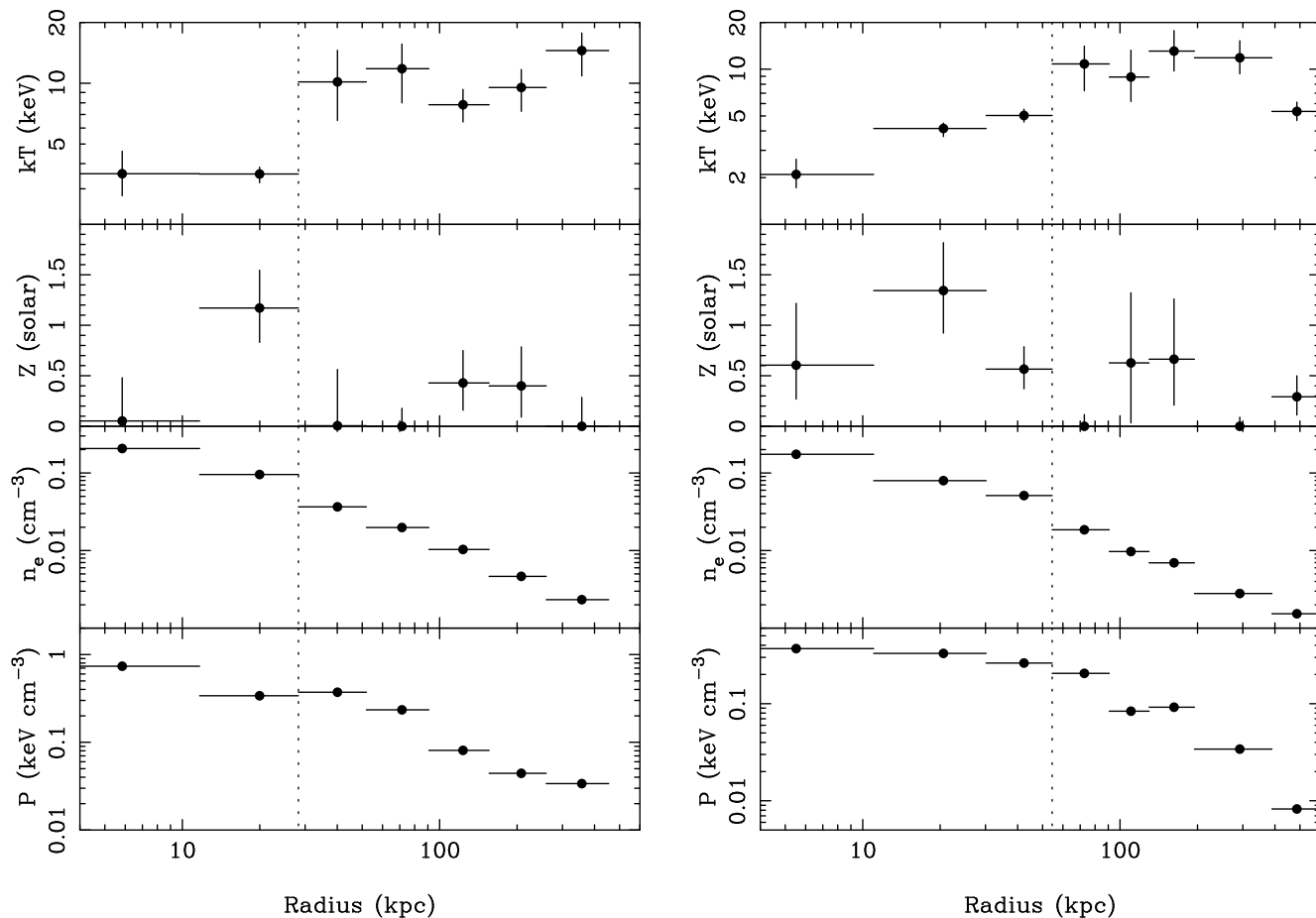


**Figure 6.** Temperature, abundance, density and pressure profiles across the two cold-fronts. The dotted line marks the radius of the cold front. (Left) The inner cold front to the north-east. (Right) The outer cold front to the west. Note that the pressure is continuous across both fronts.

each shell. The best fitting value of  $N_H$ ,  $(3.8 \pm 0.2) \times 10^{20} \text{ cm}^{-2}$ , is close to the Galactic value of  $3.2 \times 10^{20} \text{ cm}^{-2}$  (Dickey & Lockman 1990). The profiles generated from the temperature and abundance maps (Fig. 2) show very similar features to the deprojected plot. The centre of the cluster has a high electron density ( $\sim 0.2 \text{ cm}^{-3}$ ), and flat abundance and temperature profile. We can also see the ring of increased abundance and reduced temperature at a radius of  $\sim 100 \text{ kpc}$ . If we introduce a power-law component in the innermost annulus, there is no significant improvement in the quality of fit.

From the above profiles the mean radiative cooling time ( $t_{\text{cool}} = \frac{5}{2} kT n_e / L$ , where  $L$  is the luminosity per unit volume), entropy ( $S = kT n_e^{-2/3}$ ) and electron pressure ( $P = kT n_e$ ) profiles can be calculated (Fig. 8). The plot shows that the cooling time of the gas within  $\sim 10 \text{ kpc}$  is short ( $\sim 230 \text{ Myr}$ ), increasing to the age of the universe at around  $100 \text{ kpc}$ . If we include an extra MKCFLOW cooling flow model component to the innermost deprojected region (cooling from the temperature of the MEKAL component to zero, at the same abundance), a  $2\text{-}\sigma$  upper limit for the cooling flow flux is  $12 \text{ M}_\odot \text{ yr}^{-1}$ . However this value depends on the absorption used. If we allow the absorption to vary in each shell (note that this is not done in a physically-consistent way, as the absorption is not applied in projection), then there is a cooling flow limit of  $97 \text{ M}_\odot \text{ yr}^{-1}$  ( $2\text{-}\sigma$ ) in the innermost shell, with a best fitting value of  $40 \text{ M}_\odot \text{ yr}^{-1}$ . Instead of the cooling flow component we also tried an additional

powerlaw component. There was no significant reduction in the fit-statistic when the component was added.

To further constrain the amount of cooling in this cluster, we extracted a spectrum from the inner  $50 \text{ kpc}$ , and fit it with a MKCFLOW model with the abundance, upper and lower temperature free, but with the absorption fixed at the Galactic value similar to that used on other clusters (Peterson et al 2003). The best fitting model cooled from  $8.0^{+0.7}_{-1.2} \text{ keV}$  to  $2.2^{+0.5}_{-0.2} \text{ keV}$  at a rate of  $1090^{+430}_{-130} \text{ M}_\odot \text{ yr}^{-1}$  with an abundance of  $0.78 \pm 0.06 Z_\odot$ . If we introduced a further component cooling from the lower temperature of the first component to zero, we found an upper limit for the rate of cooling of  $15 \text{ M}_\odot \text{ yr}^{-1}$  ( $2\text{-}\sigma$ ). It is interesting to compare these values to Peres et al (1998) who measured fluxes of  $842^{+127}_{-82}$  and  $843^{+245}_{-152} \text{ M}_\odot \text{ yr}^{-1}$  with a surface-brightness-deprojection technique using the PSPC and HRC on *ROSAT*, and Allen (2000) who spectrally measured  $2103^{+356}_{-378} \text{ M}_\odot \text{ yr}^{-1}$  with *ASCA*.

These results indicate that the temperature distribution of the gas within the central  $50 \text{ kpc}$  is consistent with radiative cooling between  $8$  and  $2 \text{ keV}$ . Presumably some form of distributed heating is preventing a full cooling flow from developing. The lack of an accumulation of gas at a particular temperature (similar to the result found in the Perseus cluster; Sanders et al 2004) means that the heating has to operate over the full temperature range. A residual central cooling rate of at least several  $\text{M}_\odot \text{ yr}^{-1}$ , consistent with our spectra, is needed to fuel the star formation rate observed (Crawford et al 1999).

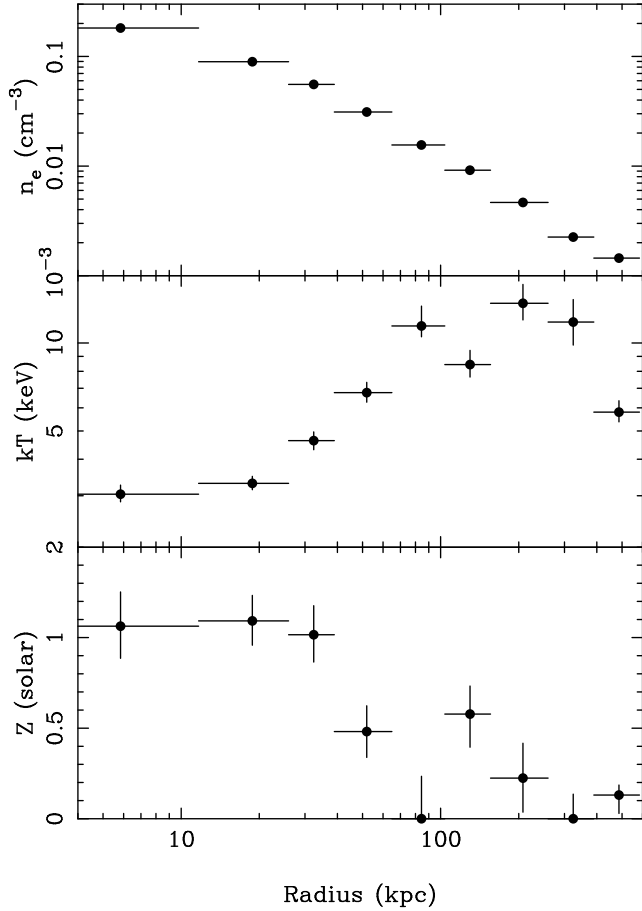


**Figure 7.** Electron density, temperature and abundance profiles in the cluster, accounting for projection. Error bars are  $1\sigma$ .

Where the temperature decreases in the outer part of the cluster ( $\sim 100$  kpc), it is interesting that the cooling time and entropy only slightly change, but the pressure decreases by a factor of 2.3. Furthermore this radius is where the cooling time reaches the age of the universe. At very large radii ( $\gtrsim 400$  kpc) the temperature of the cluster appears to drop dramatically to 6–7 keV. We do not understand the cause of this apparent drop but it appears similar to what is seen in Abell 3581 (Johnstone et al, submitted).

#### 4 DISCUSSION

There are several indications that the core of Abell 2204 is highly disturbed. There is the morphology of its centre: the flat core, the cold fronts, the central plateau, and the tail. In addition the structure of the radio source is unusual. Other evidence is provided by the cool high abundance ring at around 100 kpc and, possibly, the binary appearance of the central galaxy. Much of this can be explained by a merger event. Despite this disruption the cooling time of the centre is very short ( $\sim 230$  Myr), similar to many other centrally X-ray peaked clusters. Presumably this means that any merger was not of equal mass but with a much smaller subcluster.

The presence of two cold fronts in Abell 2204 may indicate the existence of substantial magnetic fields that suppress thermal conduction and prevent Kelvin-Helmholtz instabilities from forming (Vikhlinin, Markevitch & Murray 2001). Other indirect evidence for cluster magnetic fields in Abell 2204 is the low fractional polar-

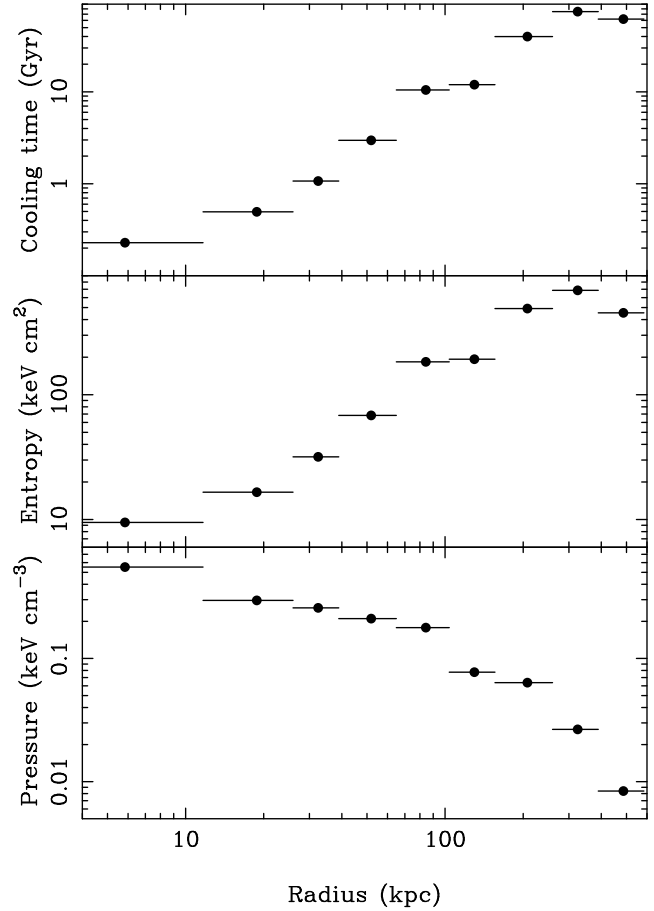


**Figure 8.** Mean radiative cooling time, entropy and electron pressure profiles of the cluster, derived from Fig. 7.

isation seen at radio wavelengths. A merger has presumably left the central galaxy/galaxies oscillating at the centre of the cluster potential, thereby making the inner and outer cold fronts either side of the central galaxy.

#### ACKNOWLEDGEMENTS

ACF thanks the Royal Society for support. The authors are grateful to Roderick Johnstone for discussions. The National Radio Astronomy Observatory is operated by Associated Universities, Inc., under cooperative agreement with the National Science Foundation.

#### REFERENCES

- Allen S.W., 2000, MNRAS, 315, 269
- Anders E., Grevesse N., 1989, Geochimica et Cosmochimica Acta, 53, 197
- Arnaud, K.A., 1996, Astronomical Data Analysis Software and Systems V, eds. Jacoby G. and Barnes J., p17, ASP Conf. Series volume 101
- Balucinska-Church M., McCammon D., 1992, ApJ, 400, 699
- Buote D.A., Tsai J.C., 1996, ApJ, 458, 27
- Cash W., 1979, ApJ, 228, 939
- Churazov E., Forman W., Jones C., Böhringer H., 2003, ApJ, 590, 225
- Clowe D., Schneider P., 2002, A&A, 395, 385
- Condon J.J., Cotton W.D., Greisen E.W., Yin Q.F., Perley R.A., Taylor G.B., Broderick J.J., 1998, AJ, 115, 1693

- Crawford C.S., Allen S.W., Ebeling H., Edge A.C., Fabian A.C., 1999, 306, 857
- Dahle H., Kaiser N., Irgens R.J., Lilje P.B., Maddox S.J., 2002, ApJS, 139, 313
- Dickey, J.M., Lockman F.J., 1990, ARA&A, 28, 215
- Edge A.C., Stewart G.C., Fabian A.C., Arnaud K.A., 1990, MNRAS, 245, 559
- Edge A.C., 2001, MNRAS, 328, 762
- Edge A.C., Wilman R.J. Johnstone R.M., Crawford C.S., Fabian A.C., Allen S.W., 2002, MNRAS, 337, 49
- Jenner D.C., 1974, ApJ, 191, 55
- Johnstone R.M., Allen S.W., Fabian A.C., Sanders J.S., 2002, MNRAS, 336, 299
- Jones C., Forman W., Vikhlinin A., Markevitch M., David L., Warmflash A., Murray S., Nulsen P.E.J. 2002, ApJ, 567, L115
- Liedahl D.A., Osterheld A.L., Goldstein W.H., 1995, ApJ, 438, L115
- Markevitch M. et al., 2000, ApJ, 541, 542
- Markevitch M., 2004, <http://hea-www.harvard.edu/~maxim/axaf/acisbg/>
- Mewe R., Gronenschild E.H.B.M., van den Oord G.H.J., 1985, A&AS, 62, 197
- Peres C.B., Fabian A.C., Edge A.C., Allen S.W., Johnstone R.M., White D.A., 1998, MNRAS, 298, 416
- Peterson J.R., Kahn S.M., Paerels F.B.S., Kaastra J.S., Tamura T., Bleeker J.A.M., Ferrigno C., Jernigan J.G., 2003, ApJ, 590, 207
- Sanders J.S., Fabian A.C., 2002, MNRAS, 331, 273
- Sanders J.S., Fabian A.C., Allen S.W., Schmidt R.W., 2004, MNRAS, 349, 952
- Schmidt R.W., Fabian A.C., Sanders J.S., 2002, MNRAS, 337, 71
- Schuecker P., Böhringer H., Reiprich T.H., Feretti L., 2001, A&A, 378, 408
- Taylor G.B., Barton E.J., Ge J., 1994, AJ, 107, 1942
- Vikhlinin A., Markevitch M., Murray S.S., 2001, ApJL, 549, L47
- Vikhlinin A., 2003, [http://asc.harvard.edu/cont-soft/software/corr\\_tgain.1.0.html](http://asc.harvard.edu/cont-soft/software/corr_tgain.1.0.html)
- Zhao J., Sumi D.M., Burns J.O., Duric N., 1993, ApJ, 416, 51